Supporting Information

A New Metal-Organic Open Framework Enabling Facile Synthesis of Carbon Encapsulated Transition Metal Phosphide/Sulfide Nanoparticle Electrocatalysts†

*Baicheng Weng, Xiaoming Wang, Corey R. Grice, Fenghua Xu, and Yanfa Yan**

* Correspondence and requests for materials should be addressed to Y.F.Y. (email: yanfa.yan@utoledo.edu).

Supporting Figures

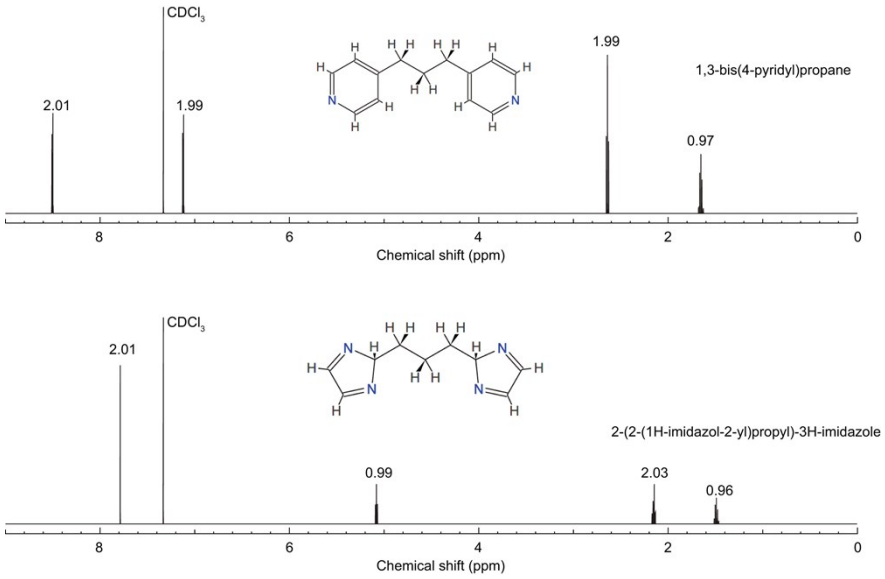

Fig. S1. ^{1}H NMR spectra of the obtained 1,3-Di(4-pyridyl)propane and 2-(2-(1H-imidazol-2-yl)propyl)-

3H-imidazole.

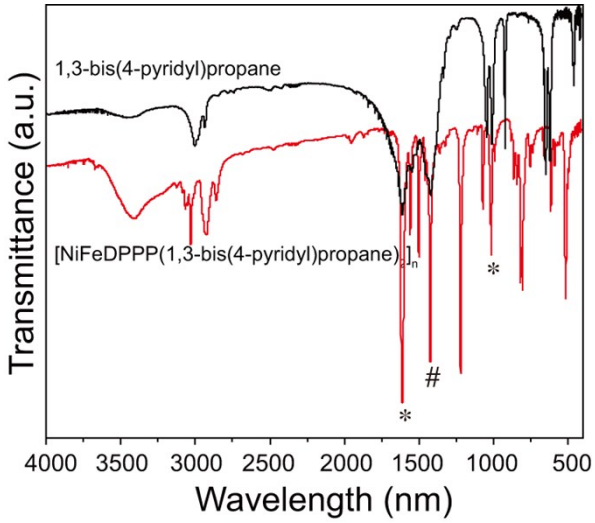

Fig. S2. FTIR patterns of the obtained 1,3-Di(4-pyridyl)propane (black curve) and [NiFeDPPP(1,3-Di(4-pyridyl)propane)$_2$]$_n$ (red curve). Asterisks: characteristic peaks of pyridine rings. Double-cross: characteristic peak of phenylphosphine groups.

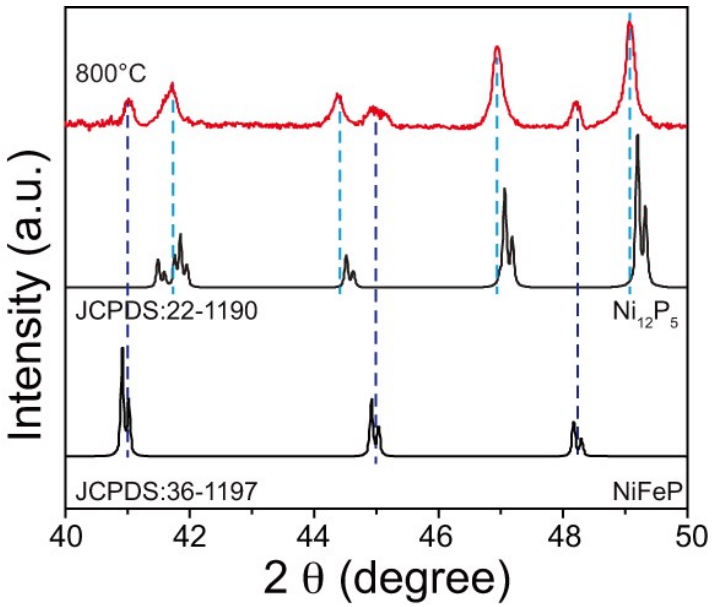

Fig. S3. XRD patterns of NiP/NiFeP/C between 40° and 50°. Reference diffraction patterns of standard $Ni_{12}P_5$ and NiFeP are also labeled.

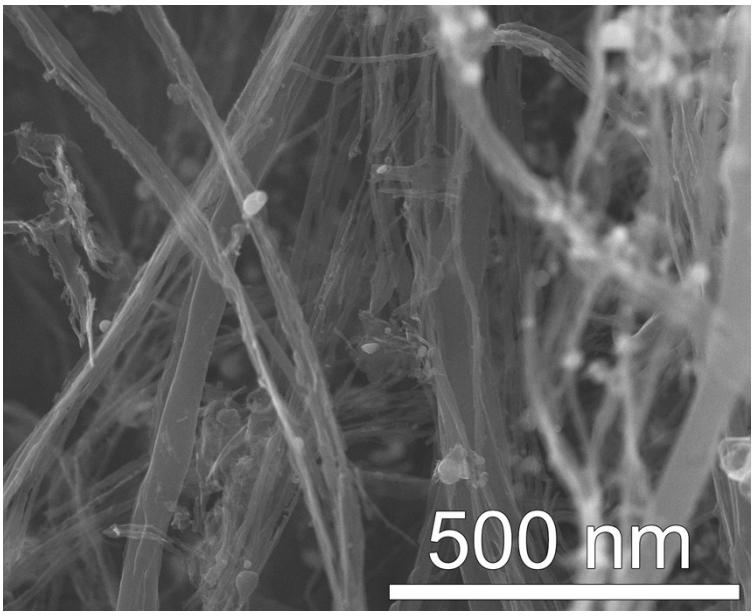

Fig. S4. SEM image of the obtained NiP/NiFeP/C, showing the carbon fibers.

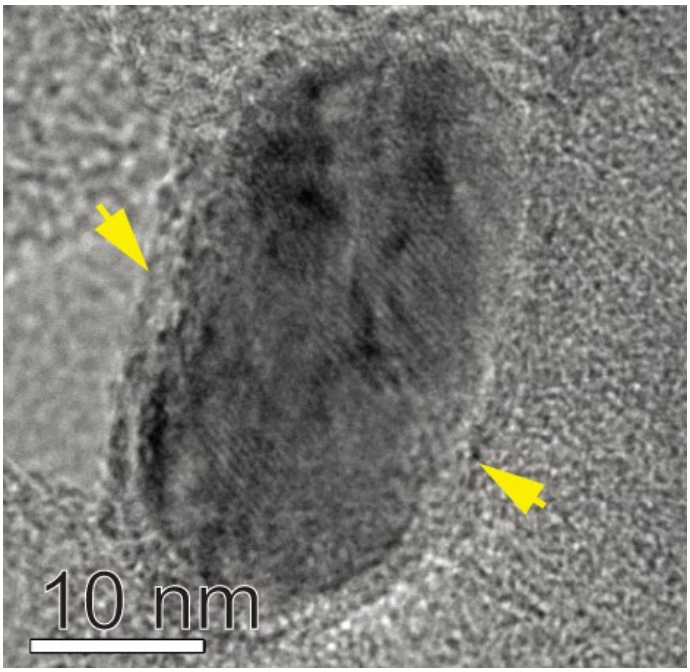

Fig. S5. TEM image of the obtained NiP/NiFeP/C. Yellow arrows show the amorphous shell the nanoparticle.

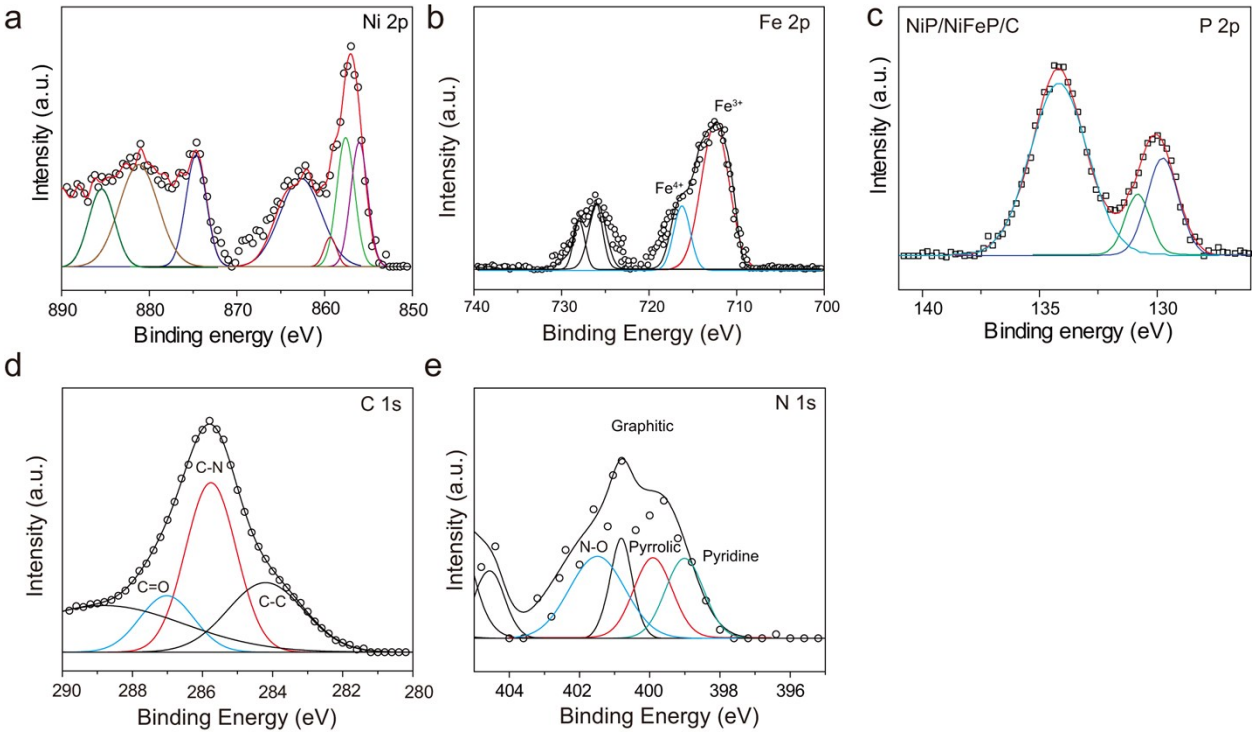

Fig. S6. XPS spectra of the Ni 2p, Fe 2p, P 2p, C 1s, and N 1s core-levels of NiP/NiFeP/C.

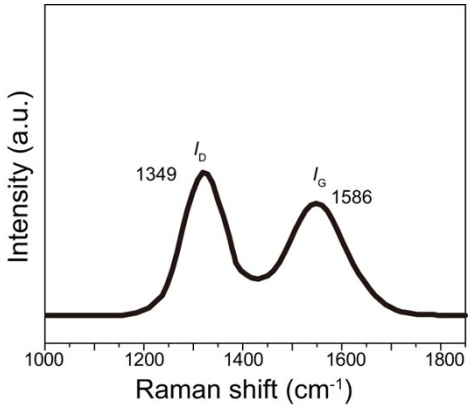

Fig. S7. Raman spectrum of NiP/NiFeP/C. The peak positions (1349 and 1586 cm^{-1}) corresponding to *D* and *G* bands of heteroatom-doped carbon are also labeled.

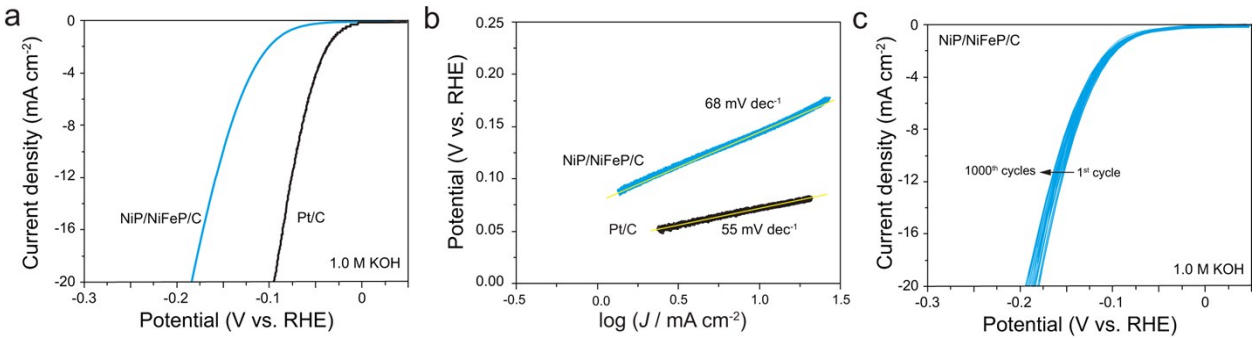

Fig. S8. HER performance of NiP/NiFeP/C and Pt/C in 1.0 M KOH. (a) Polarization curves. (b) Corresponding Tafel slopes. (c) Stability test of NiP/NiFeP/C for 1000 HER cycles. Pt/C (commercial Pt/C, 20% Pt) was compared as a reference. Pt/C shows an onset potential of 0 mV and achieves a stable current density of -10 mA cm^{-2} at a potential of -73 mV (vs. RHE) in 1.0 M KOH.[S1, S2]

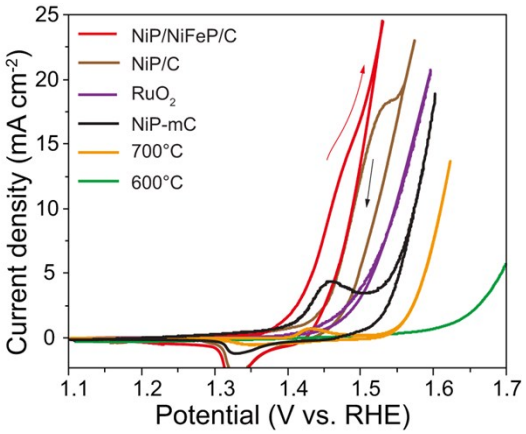

Fig. S9. Cyclic volumetric curves with both positive and negative scans of NiP/NiFeP/C and the samples obtained by pyrolysis of Ni, Fe-MOF at 600 °C and 700 °C for OER in 1.0 M KOH. RuO_2, NiP/C and NiP-mC are also added for comparisons.

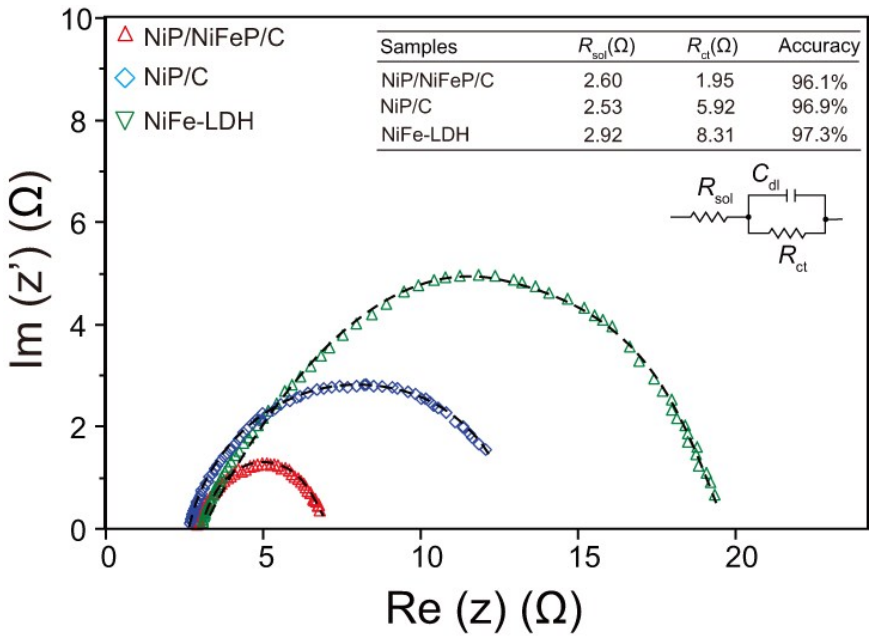

Fig. S10. EIS curves of the NiP/NiFeP/C, NiP/C, and NiFe-LDH samples. Inserted circuit model: R_{sol}: resistance of solution, R_{ct}: charge transfer resistance, C_{dl}: double-layer capacitance. Dash lines are the fitting curves according to the inserted circuit model. Inserted table shows equivalent circuit parameters obtained from EIS measurements.

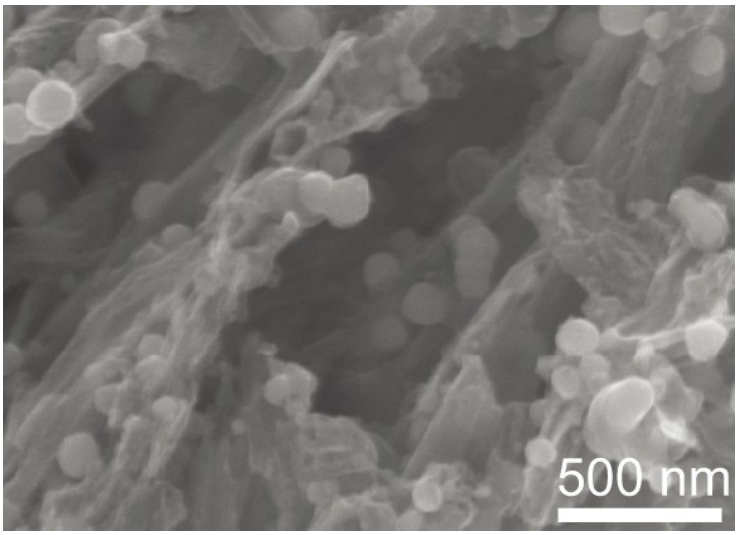

Fig. S11. SEM image of NiP/NiFeP/C after stability test.

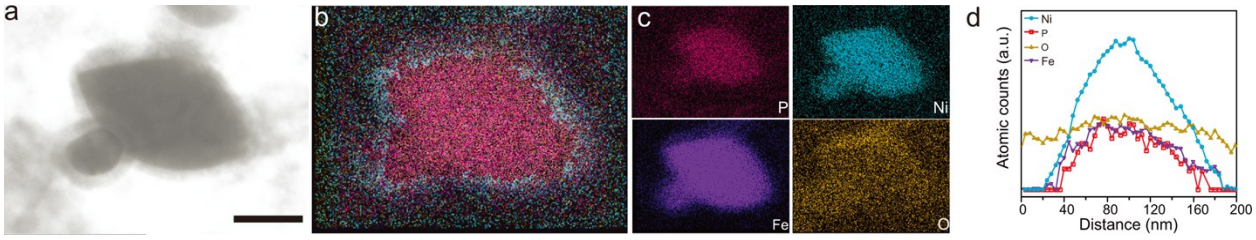

Fig. S12. STEM-EDS elemental mapping and linear scanning of the NiP/NiFeP/C after stability test. (a) STEM image. (b) Overlapping of elemental mapping. (c) P, Ni, Fe, and O elemental mapping. (d) Linear scanning of the NiP/NiFeP/C sample. Scale bar: 100 nm.

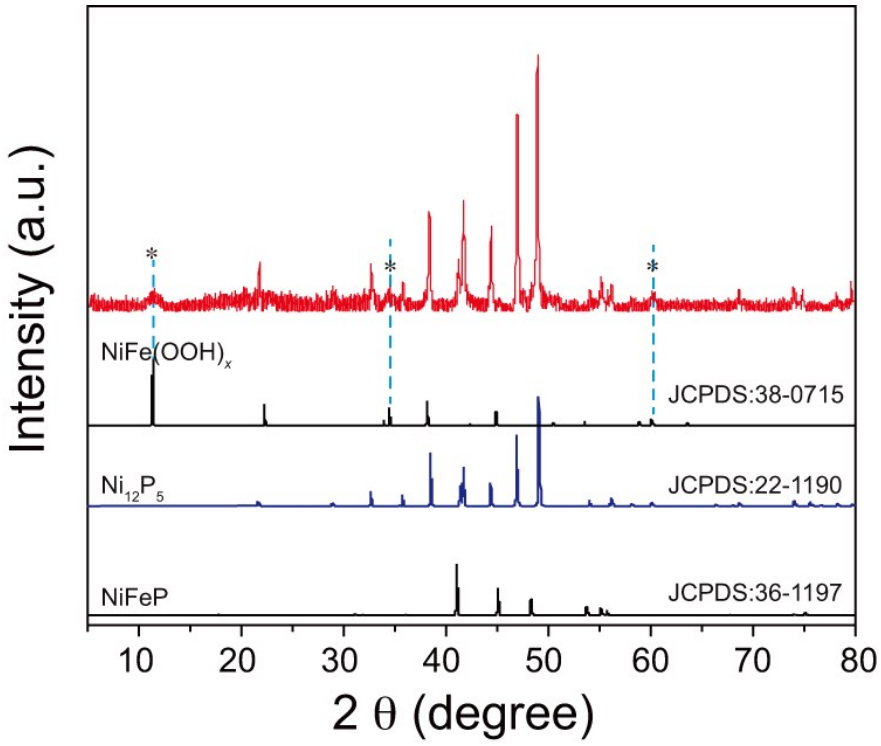

Fig. S13. XRD pattern of the NiP/NiFeP/C after stability test. The dash lines are added for eye.

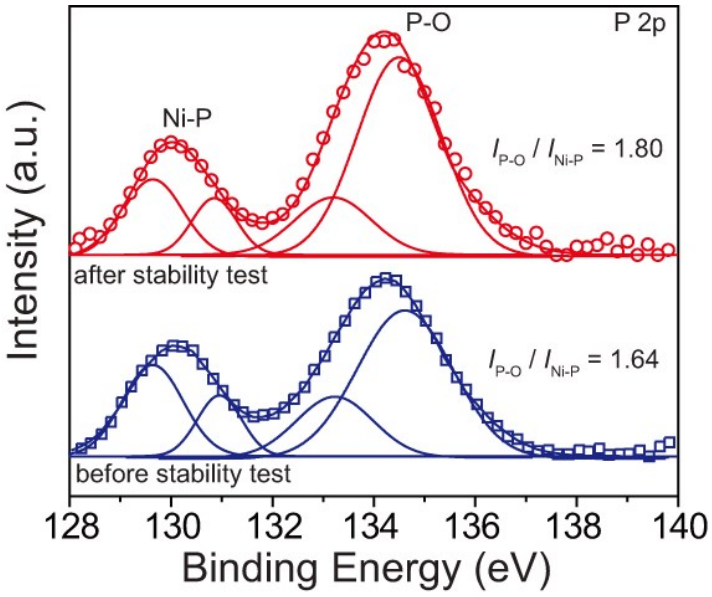

Fig. S14. XPS P 2p core-level of the NiP/NiFeP/C after stability test.

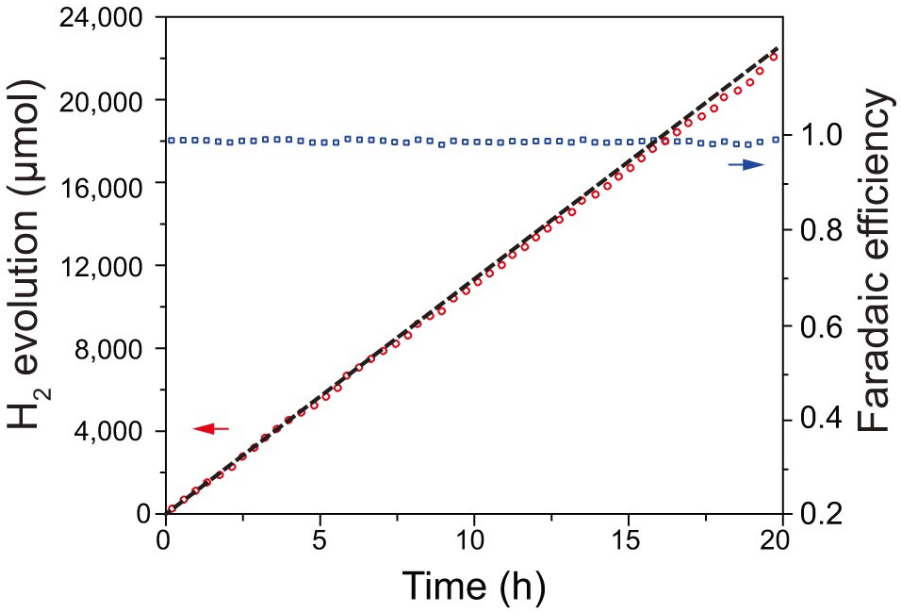

Fig. S15. Hydrogen evolution rate and Faradaic efficiency from gas chromatography measurement for the bifunctional NiP/NiFeP/C catalyst in a two-electrode overall water splitting system.

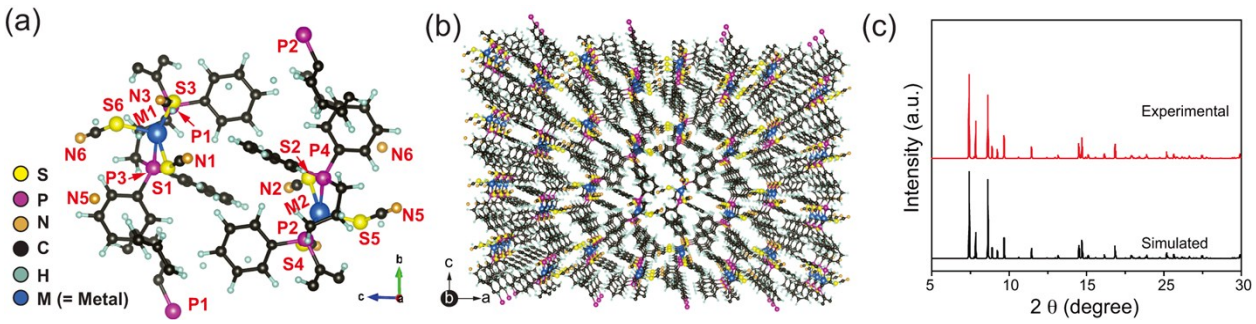

Fig. S16. (a) Unit-cell content of the crystal structure of the Mo, W-MOF with atoms labeled. Hydrogen and carbon atoms are not labeled for clarity. (b) The crystal structure of Mo, W-MOF with 4 × 4 × 3 unit cells (b × c × a). (c) Experimental and simulated XRD patterns of Mo, W-MOF.

Compared to Ni, Fe-MOF, the Mo, W-MOF uses the thiocyanate rather than 1,3-bis(4-pyridyl)propane linkers to reduce the carbon content and introduce S into the obtained electrocatalyts. Each Mo/W atom coordinates three N atoms, three S atoms, and two P atoms, while adjacent TM atoms are separated with at least two benzene rings. The experimental and simulated XRD patterns match closely, indicating a high crystal purity for the synthesized samples.

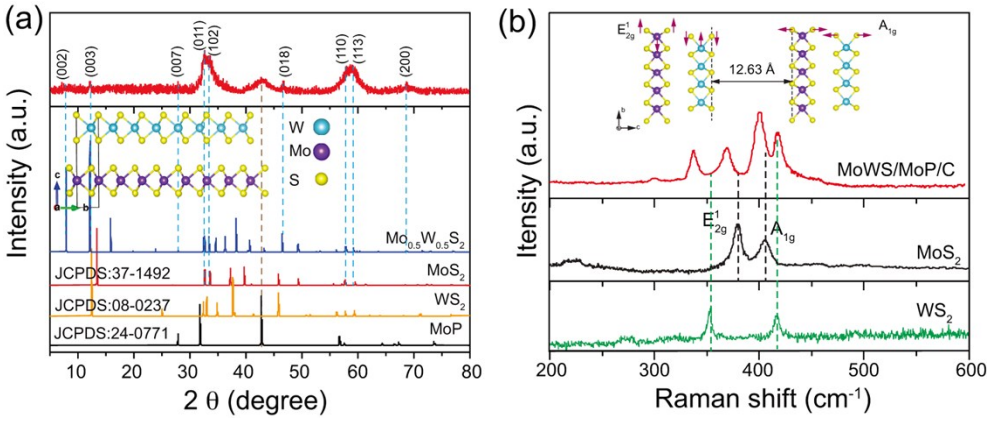

Fig. S17. (a) XRD patterns of MoWS/MoP/C, and reference diffraction patterns of standard $Mo_{0.5}W_{0.5}S_2$, WS_2, MoS_2, and MoP are also labeled. c) Raman spectra of MoWS/MoP/C and WS_2, MoS_2. Inserted images in (a) and (b): crystal structure of $Mo_{0.5}W_{0.5}S_2$.

The structure of $Mo_{0.5}W_{0.5}S_2$ is similar to its counterpart, 2H-MoS_2. In one layer, a plane of Mo (or W) atoms is sandwiched covalently between two planes of S atoms in a trigonal prismatic arrangement. The

interaction between layers is dominated by van der waal forces. Each hexahedral layer of 2H-MoS_2 is sandwiched by two layers of 2H-WS_2 hexahedral layers (**Fig. S17a and S17b,** inserted images) with different interlayer spacing of ~ 4 Å and ~ 12.6 Å. While the interlayer spacing of 2H-MoS_2 is 4.6 Å.[S3] It is believed that increasing the interlayer spacing of MoS_2 will tune its electronic structure, and more than 7% expansion will be treated as a two-dimensional single-layer model.[S4] Further Raman characterizations (**Fig. S17b**) confirm the XRD analysis. Raman spectrum of MoWS/MoP/C exhibits four distinct peaks at 417.9, 400.0, 368.8, and 339.1 cm^{-1}, and the peaks located at 400.0 and 368.8 cm^{-1} correspond to the out-of-plane Mo–S phonon mode (A_{1g}) and the in-plane Mo–S mode (E^1_{2g}) of typical MoS_2-layered structure, respectively. While the peaks located at 417.9 and 339.1 cm^{-1} are ascribed to the A_{1g} and E^1_{2g} of typical WS_2-layered structure, respectively.[S5] The Raman spectra also show red-shift of the A_{1g} and E^1_{2g} peaks, which results from the greatly expanded interlayer spacing. Notably, compared to Raman spectra of pristine MoS_2 and WS_2, the integrated intensity of A_{1g} is almost 3.5 times higher than that of E^1_{2g}, so the obtained MoWS/MoP/C sample favors the vibration of A_{1g} mode and displays the highly exposed edge sites.

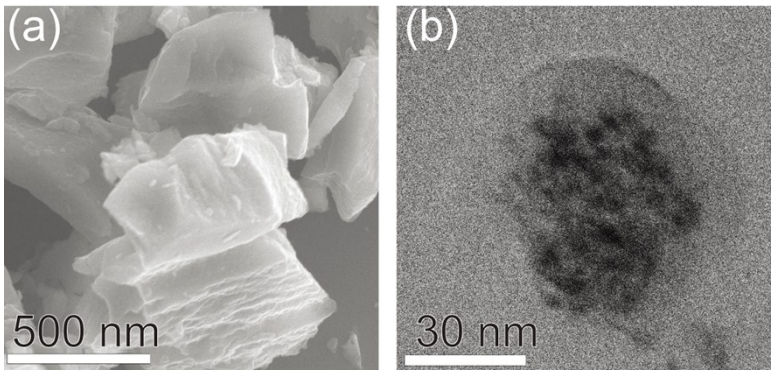

Fig. S18. SEM (a) and TEM (b) images of the obtained MoWS/MoP/C.

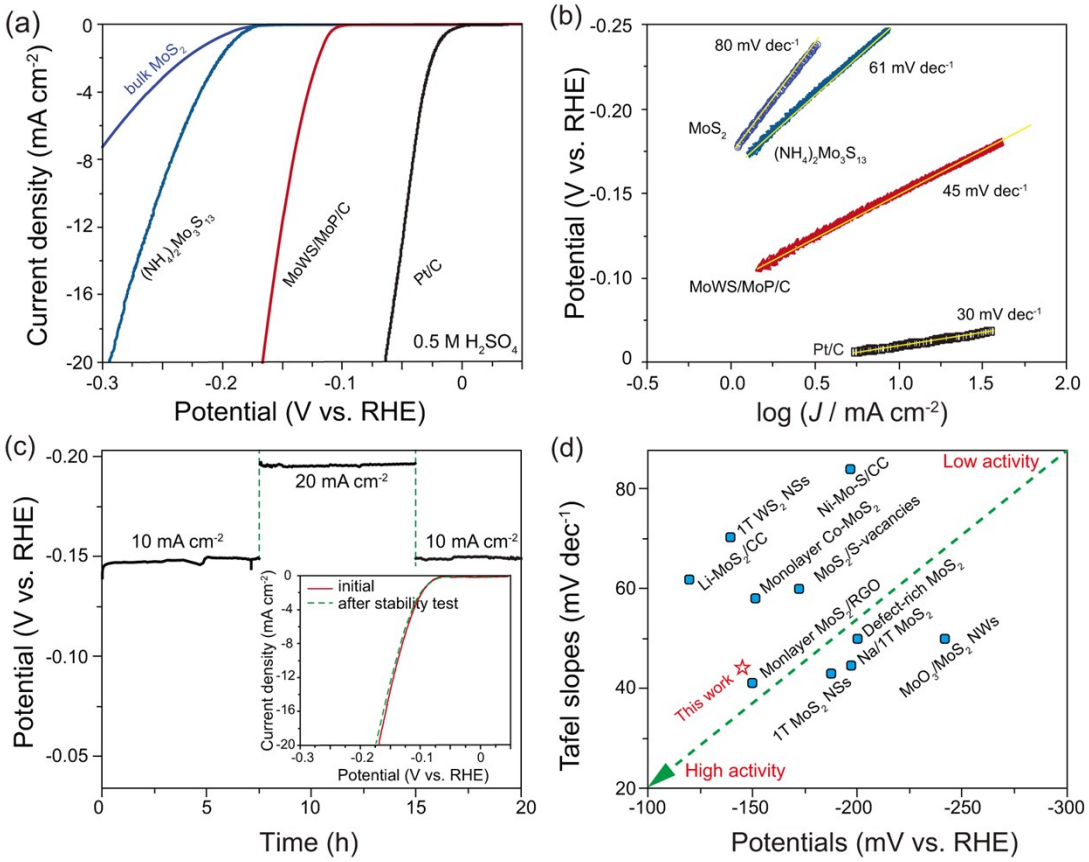

Fig. S19. (a) Polarization curves of MoWS/MoP/C, MoS_2, and $(NH_4)_2Mo_3S_{13}$ for HER in 0.5 M H_2SO_4. (b) Corresponding Tafel plots. (c) Durability test for MoWS/MoP/C sample at -10 mA cm^{-2} and -20 mA cm^{-2} for 20 h and its corresponding polarization curves (inserted plot). (d) Comparison of the electrochemical activities (Tafel slopes and potentials at -10 mA cm^{-2}) with the reported MoS_2 nanostructures, such as Li-MoS_2/CC,[S6] 1T-WS_2 NSs,[S7] Ni-Mo-S/CC,[S8] monolayer Co-MoS_2/CC,[S9] MoS_2/S-vacancies,[S10] monolayer MoS_2/rGO,[S11] Na/1T-MoS_2,[S12] Defect-rich MoS_2,[S13] MoO_3/MoS_2 NWs,[S14] and 1T-MoS_2 NSs.[S15] CC: carbon cloth, NWs: nanowires, NSs: nanosheets.

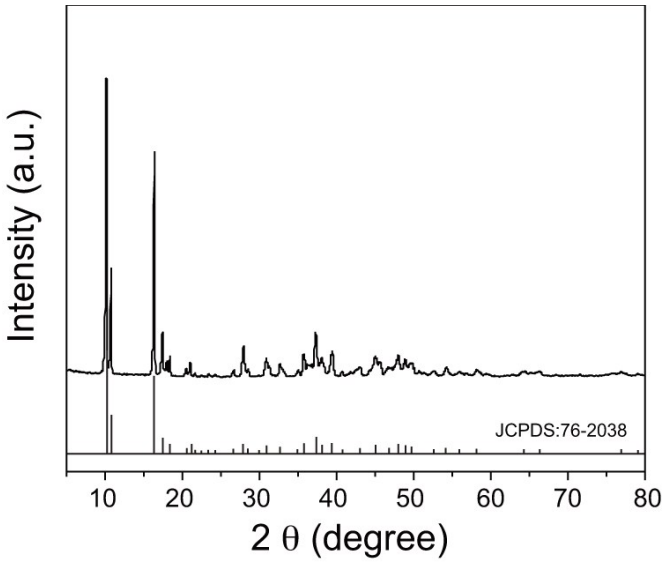

Fig. S20. XRD pattern of the synthesized $(NH_4)_2Mo_3S_{13}•nH_2O$ with a reference spectrum displayed at the bottom (Joint Commission for Powder Diffraction Standards (JCPDS): #76-2038).

Table S1 Comparison of HER performance for NiP/NiFeP/C with other reported non-noble electrocatalysts in 0.5 M H_2SO_4.

Samples	Potential (mV vs. RHE) at 10 mA cm^{-2}	Loading amount (mg cm^{-2})	Tafel slope (mV dec^{-1})	References
NiP/NiFeP/C	-87	0.168	38	*This work*
S-CoWP@(S,N)-C	-35	0.75	35	*ACS Energy Lett.*, ***2018***, *3, 1434–1442.*
CoPS NSs on carbon cloth	-48	N/A	56	*Nature Materials, 2015, 14, 1245-1251*
WP nanowires on carbon cloth	-130	2.00	69	*ACS Appl. Mater. Interfaces 2014, 6, 21874*
P-Mo_2C/C	-89	1.30	42	*Energy Environ. Sci. 2017,10, 1262-1271*
EG/$Co_{0.85}Se$/NiFe-LDH	-225	4.00	160	*Energy Environ. Sci. 2016, 9, 478--483*
Ultrathin $NiFeS_x$ nanosheets	-107	25±2	40	*J. Am. Chem. Soc. 2015, 137, 11900−11903*
$CoWS_x$	-238	N/A	N/A	*Energy Environ. Sci.*

				2013, 6, 2452–2459
WP NPs@NC	-102	2.0	58	*J. Mater. Chem. A 2016, 4, 15327*
P-WN/rGO	-85	0.34	54	*Angew. Chem. Int. Ed. 2015, 54, 6325 –6329*
MoP|S	-64	1.00	N/A	*Angew. Chem. 2014, 126, 14661 –14665*
MPSA/GO	-163	0.30	89	*Angew. Chem. Int. Ed. 2016, 55, 2230 –2234*
MoS_2 sheet stacks	-106	3.00	59	*Energy Environ. Sci. 2017,10, 593-603*
$NiP_{1.93}Se_{0.07}$/GD	-102	N/A	42	*ACS Catal. 2015, 5, 6355−6361*
Co-NG	-147	0.29	82	*Nat. Commun. 2015, 6:8668*

Table S2 Electrochemical properties of NiP-mc, NiP/NiFeP/C, and NiP/C samples.

Samples	C_{dl} (mF cm^{-2})	$J_{0,geometrical}$ (mA cm^{-2})	$J_{0,normalized}$ (mA cm^{-2})
NiP-mc	51.4	0.486	0.009
NiP/NiFeP/C	35.9	0.723	0.020
NiP/C	32.3	0.402	0.012

Table S3 Comparison of HER performance for NiP/NiFeP/C with other reported non-noble electrocatalysts in 1.0 M KOH.

Samples	Potential (mV vs. RHE) at -10 mA cm^{-2}	Loading amount (mg cm^{-2})	Tafel slope (mV dec^{-1})	References
NiP/NiFeP/C	-138	0.168	68	*This work*
S-CoWP@(S,N)-C	-61	0.75	61	*ACS Energy Lett.*, ***2018***, *3, 1434–1442.*
2.5H-PHNCMs	-70	1.00	38.1	*Nat. Commun. 2017, 8,*

				15377
EG/$Co_{0.85}Se$/NiFe-LDH	-260	4.00	160	*Energy Environ. Sci. 2016, 9, 478--483*
Ni/NiP	-130	10.58-11.04	58.5	*Adv. Funct. Mater. 2016, 26, 3314–3323*
CoP nanowires on carbon cloth	-210	0.92	51	*J. Am. Chem. Soc. 2014, 136, 7587*
WP nanowires on carbon cloth	150	2.00	102	*ACS Appl. Mater. Interfaces 2014, 6, 21874*
NiFe-LDH	-210	N/A	N/A	*Science 2014, 345, 1593*
MOF derived MoC_x	-151	0.14	59	*Nat. Commun. 2016, 6, 6512*
N,S-CNT	-450	N/A	133	*Adv. Energy Mater. 2017, 1602068*
CoO_x/CN	-270	0.85	115	*J. Am. Chem. Soc. 2015, 137, 2688*
CP/CTs/Co-S	-190	0.32	101	*ACS Nano, 2016, 2342–2348*
PCPTF	-370	0.10	53	*Adv. Mater. 2015, 27, 3175–3180*
Co_9S_8@MoS_2/CNFs	-190	0.212	110	*Adv. Mater. 2015, 27, 4752–4759*

Table S4 Comparison of OER performance for NiP/NiFeP/C with recently reported catalysts in alkaline solution.

Samples	Potential (V vs. RHE) at 10 mA cm^{-2}	Tafel slope (mV dec^{-1})	TOF (s^{-1})	Loading amount (mg cm^{-2})	References
NiP/NiFeP/C*	1.48	58	0.133 @1.51 V	0.168	*This work*
NiFe-LDH-rGO	1.53	82	0.1 @ 1.53V	0.25	*ACS Nano* **2015**, 9, 1977-1984
G-FeCoW# on Au coated nickel foam	1.45	N/A	0.46 @1.53 V	0.21	*Science* **2016**, *352, 333-337*

CoNi-P on nickel foam	1.50	52	N/A	0.153	*Energy Environ. Sci.* **2017**, 10, 893-899
$NiCeO_x$ on Au	1.50	N/A	0.08 @1.51 V	~0.13	*Nature Energy* **2016**, 1, 16053
Ni_2P/Ni on nickel foam[#]	1.43	N/A	0.015 @1.58 V	N/A	*ACS Catal.* **2016**, 6, 714−721
$NiPS_3$@NiOOH	1.58	80	N/A	0.126	*ACS Catal.* **2017**, 7, 229−237
LT-$LiCoO_2$	1.66	48	N/A	0.32	*Energy Environ. Sci.* **2016**,9, 184-192
NiD-PCC	1.59	98	N/A	N/A	*Energy Environ. Sci.* **2016**, 9, *3411-3416*
Ni_3Se_2	1.54	97	N/A	0.217	*Energy Environ. Sci.* **2016**, 9, 1771--1782
FeNi@NC	1.51	70	N/A	0.32	*Energy Environ. Sci.* **2016**, 9, 123--129
Ni–P nanoplates	1.53	64	N/A	0.20	*EnergyEnviron.Sci.* **2016**, 9, 1246--1250
De-LCoP@5.1 V	1.654	73	N/A	0.50	*Energy Environ. Sci.* **2015**, 8, 1719--1724
LT-$LiCoO_2$	1.61	52	N/A	0.25	*Nat. Commun.* **2014**, 5, 3949
$LiNi_{0.8}Al_{0.2}O_2$	1.58	44	N/A	0.051	*Adv. Mater.* ***2015****, 27, 6063–6067*
NiV-LDH	1.55	64	0.054 @1.58 V	0.143	*Nat. Commun.* **2016**, 7, 11981
CoMn-LDH	1.53	43	0.075 @ 1.53V	0.222	*J. Am. Chem. Soc.* ***2014****, 136, 16481-16484*
NiCo-LDH	1.62	59	0.05 @ 1.53V	0.07	*Nat. Commun.* **2014**, 5, 4477
NiFe*	1.65	N/A	0.075 @1.63 V	N/A	*Nat. Commun.* **2015**, 6, 6616
Co_3O_4/rm-GO	1.54	67	N/A	0.17	*Nat. Mater.* **2011**, 10, 780
N-doped graphene-CoO	1.57	71	N/A	N/A	*Energy Environ. Sci.* **2014**, 7, 609

* on glassy carbon; [#] TOF estimated according to electrochemical active sites not all the metal cations.

References

[S1] Z. Shi, K. Nie, Z. J. Shao, B. Gao, H. Lin, H. Zhang, B. Liu, Y. Wang, Y. Zhang, X. Sun, *Energy Environ. Sci*. **2017**,*10*, 1487.

[S2] M. Cabán-Acevedo, M. L. Stone, J. R. Schmidt, J. G. Thomas, Q. Ding, H. C. Chang, M. L. Tsai, J. H. He, J. Jin, *Nat. mat.* **2015**, *14*, 1245.

[S3] B. Hinnemann, P.G. Moses, J. Bonde, K.P. Jørgensen, J.H. Nielsen, S. Horch, I. Chorkendorff, J. K. Nørskov, *J. Am. Chem. Soc*. **2005**, *127*, 5308.

[S4] K. Kobayashi, J. Yamauchi, *Phys. Rev. B* **1995**, *51*, 17085.

[S5] N. H. Attanayake, A. C. Thenuwara, A. Patra, Y. V. Aulin, T. M. Tran, H. Chakraborty, E. Borguet, M. L. Klein, J. P. Perdew, D. R. Strongin, *ACS Energy Lett*. **2018**, *3*, 7.

[S6] H. Wang, Z. Lu, S. Xu, D. Kong, J. J. Cha, G. Zheng, P. C. Hsu, K. Yan, D. Bradshaw, F. B. Prinz, Y. Cui, *PNAS*. **2013**, *110*, 19701.

[S7] M. A. Lukowski, A. S. Daniel, C. R. English, F. Meng, A. Forticaux, R. J. Hamers, S. Jin, *Energy Environ. Sci*. **2014**, *7*, 2608.

[S8] J. Miao, F. X. Xiao, H. B. Yang, S. Y. Khoo, J. Chen, Z. Fan, Y. Y. Hsu, H. M. Chen, H. Zhang, B. Liu, *Sci. Adv*. **2015**, 1, e1500259.

[S9] X. Hai, W. Zhou, S. Wang, H. Pang, K. Chang, F. Ichihara, J. Ye, *Nano Energy* **2017**, *39*, 409.

[S10] H. Li, C. Tsai, A. L. Koh, L. Cai, A. W. Contryman, A. H. Fragapane, J. Zhao, H. S. Han, H. C. Manoharan, F. Abild-Pedersen, *Nat. Mater*. **2016**, *15*, 48.

[S11] Y. Li, H. Wang, L. Xie, Y. Liang, G. Hong, H. Dai, *J. Am. Chem. Soc*. **2011**, *133*, 7296.

[S12] N. H. Attanayake, A. C. Thenuwara, A. Patra, Y. V. Aulin, T. M. Tran, H. Chakraborty, E. Borguet, M. L. Klein, J. P. Perdew, D. R. Strongin, *ACS Energy Lett*. **2018**, *3*, 7.

[S13] J. Xie, H. Zhang, S. Li, R. Wang, X. Sun, M. Zhou, J. Zhou, X. W. Lou, Y. Xie, *Adv. Mater*. **2013**, *25*, 5807.

[S14] Z. Chen, D. Cummins, B. N. Reinecke, E. Clark, M. K. Sunkara, T. F. Jaramillo, *Nano Lett.* **2011**, *11*, 4168.

[S15] M. A. Lukowski, A. S. Daniel, F. Meng, A. Forticaux, L. Li, S. Jin, *J. Am. Chem. Soc*. **2013**, *135*, 10274.